2009

Contribution Of Impaired Myocardial Insulin Signaling To Mitochondrial Dysfunction And Oxidative Stress In The Heart

Sihem Boudina
University of Utah School of Medicine

Heiko Bugger
University of Utah School of Medicine

Sandra Sena
University of Utah School of Medicine

Brian T. O'Neill
University of Utah School of Medicine

Vlad G. Zaha
University of Utah School of Medicine

See next page for additional authors

Published in final edited form as:
Circulation. 2009 March 10; 119(9): 1272–1283. doi:10.1161/CIRCULATIONAHA.108.792101.

CONTRIBUTION OF IMPAIRED MYOCARDIAL INSULIN SIGNALING TO MITOCHONDRIAL DYSFUNCTION AND OXIDATIVE STRESS IN THE HEART

Sihem Boudina, Ph.D.[1], **Heiko Bugger, M.D. Ph.D.**[1], **Sandra Sena, Ph.D.**[1], **Brian T. O'Neill, MD. Ph.D.**[1], **Vlad G. Zaha, MD Ph.D.**[1], **Olesya Ilkun, MS.**[1], **Jordan J. Wright, BS.**[1], **Pradip K. Mazumder, DVM Ph.D.**[1], **Eric Palfreyman, MD.**[1], **Timothy J. Tidwell**[1], **Heather Theobald, BS.**[1], **Oleh Khalimonchuk, Ph.D.**[2], **Benjamin Wayment, BS**[3], **Xiaoming Sheng, Ph.D.**[4], **Kenneth J. Rodnick, Ph.D.**[5], **Ryan Centini, BS**[6], **Dong Chen, Ph.D**[6], **Sheldon E. Litwin, MD.**[3], **Bart E. Weimer, Ph.D.**[6], and **E. Dale Abel, MB.BS., D.Phil.**[1,2]

[1]Division of Endocrinology, Metabolism and Diabetes and Program in Molecular Medicine, University of Utah School of Medicine, Salt Lake City, UT

[2]Department of Biochemistry, University of Utah School of Medicine, Salt Lake City, UT

[3]Division of Cardiology, University of Utah School of Medicine, Salt Lake City, UT

[4]Department of Family and Preventive Medicine, University of Utah School of Medicine, Salt Lake City, UT

[5]Department of Biological Sciences, Idaho State University, Pocatello, ID

[6]Center for Integrated BioSystems, Utah State University, Logan, UT

Abstract

Background—Diabetes-associated cardiac dysfunction is associated with mitochondrial dysfunction and oxidative stress, which may contribute to LV dysfunction. The contribution of altered myocardial insulin action, independently of associated changes in systemic metabolism is incompletely understood. The present study tested the hypothesis that perinatal loss of insulin signaling in the heart impairs mitochondrial function.

Methods and Results—In 8-week-old mice with cardiomyocyte deletion of insulin receptors (CIRKO), inotropic reserves were reduced and mitochondria manifested respiratory defects for pyruvate that was associated with proportionate reductions in catalytic subunits of pyruvate dehydrogenase. Progressive age-dependent defects in oxygen consumption and ATP synthesis with the substrates glutamate and the fatty acid derivative palmitoyl carnitine (PC) were observed. Mitochondria were also uncoupled when exposed to PC due in part to increased ROS production and oxidative stress. Although proteomic and genomic approaches revealed a reduction in subsets of genes and proteins related to oxidative phosphorylation, no reduction in maximal activities of mitochondrial electron transport chain complexes were found. However, a disproportionate reduction in TCA cycle and FA oxidation proteins in mitochondria, suggest that defects in FA and pyruvate metabolism and TCA flux may explain the mitochondrial dysfunction observed.

Corresponding author: E. Dale Abel, Address: Division of Endocrinology, Metabolism and Diabetes, Program in Molecular Medicine, 15 N 2030 E Bldg # 533 Rm. 3110B, Salt Lake City, Utah 84112, Phone: (801) 585-0727; Fax: (801) 585-0701, dale.abel@hmbg.utah.edu.

CONFLICT OF INTERESTDISCLOSURES

(None).

Conclusions—Impaired myocardial insulin signaling promotes oxidative stress and mitochondrial uncoupling, which together with reduced TCA and FA oxidative capacity impairs mitochondrial energetics. This study identifies specific contributions of impaired insulin action to mitochondrial dysfunction in the heart.

Keywords

Metabolism; Mitochondria; Oxidative Stress; Insulin

INTRODUCTION

Recent studies have suggested that impaired mitochondrial energetics may contribute to cardiac dysfunction in obesity and diabetes [1–7]. The pathogenesis of mitochondrial dysfunction in obesity or diabetes-related heart disease is likely multifactorial, but includes fatty acid mediated mitochondrial uncoupling and oxidative damage [3, 4, 8–11]. A commonly associated finding in the heart in experimental models of obesity and diabetes is myocardial insulin resistance [12–16]. However it is not known if myocardial insulin resistance *per se* directly contributes to the pathogenesis of myocardial mitochondrial dysfunction.

The effects of myocardial insulin signaling on the acute regulation of myocardial metabolism is well known [17, 18], and includes increasing glucose uptake and glycolysis via regulation of GLUT4 translocation[19, 20] and activation of 6-phosphofructo-1-kinase (PFK-1) [21]. In perfused hearts, insulin increases glucose oxidation and reduces fatty acid (FA) oxidation[13]. *In vivo*, the antilipolytic effect of insulin also reduces the delivery of free fatty acids (FFA) to the heart, which further reduces myocardial FA oxidation [18]. The direct effects of reduced insulin signaling on myocardial substrate utilization are not well understood, in part because systemic insulin deficiency or insulin resistance will increase the delivery of FA to the heart *in vivo*, which will increase myocardial FA utilization and activate PPAR-alpha mediated transcriptional pathways that further augment myocardial FA oxidative capacity [22]. In contrast, perinatal loss of insulin receptors in cardiomyocytes reduces myocardial glucose and FA oxidation [23] suggesting that the direct effect of insulin deficiency on myocardial substrate utilization is distinct from effects that are secondary to loss of insulin signaling in the periphery.

The present study sought to elucidate direct effects of impaired insulin action on cardiac mitochondria in the absence of systemic metabolic disturbances that accompany insulin resistance or insulin deficiency. Thus, we examined mitochondrial function in mice with perinatal loss of insulin receptors in cardiomyocytes (CIRKO) to test the hypothesis that impaired myocardial insulin action might contribute to mitochondrial dysfunction in the heart in insulin resistant states. This study demonstrates that genetic deletion of insulin receptors in cardiomyocytes impairs mitochondrial function via multiple mechanisms that include loss of TCA cycle and beta-oxidation proteins, oxidative stress and mitochondrial uncoupling. Thus impaired myocardial insulin signaling might directly contribute to mitochondrial dysfunction in conditions such as obesity and diabetes.

MATERIALS AND METHODS

The authors have full access to and take full responsibility for the integrity of the data. All authors have read and agree to the manuscript as written.

Generation of mice

Mice with cardiomyocyte-selective ablation of the insulin receptor (CIRKO), generated as previously described [23] were fed standard chow (see supplementary materials for composition of chow) and housed in temperature-controlled facilities with a 12-h light and 12-h dark cycle

(lights on at 06:00). Animals were studied in the random fed state during the day (between 07:00 to 13:00) using protocols that were approved by the Institutional Animal Care and Use Committee of the University of Utah.

Determination of cardiac function by echocardiography

Echocardiography was performed in lightly anesthetized (isoflurane) mice using a Vivid7 echocardiogram unit (General Electric, Tampa, Fl), by an investigator blinded to genotype and analyzed as previously described [23–25].

Cardiac function MVO_2 and substrate utilization in perfused mouse hearts

Retrograde heart perfusions were performed in 8-, 24- and 54- week-old mice as previously described [3] with Krebs buffer containing (in mmol/l) 118 NaCl, 4.7 KCl, 25 $NaHCO_3$, 1.2 $MgSO_4$, 1.2 KH_2PO_4, 2 $CaCl_2$, and 11 glucose gassed with 95% O_2 and 5% CO_2. Heart rates were maintained at 360 beats/min by pacing at 6 Hz at the level of the atria. Oxygen consumption was calculated as previously described [3]. 8-week-old mouse hearts were also subjected to calcium-induced inotropic stress using our previously described protocols [3]. Palmitate oxidation rates and MVO_2 were determined in isolated working hearts as previously described [13].

Mitochondrial respiration and ATP synthesis

Mitochondrial function (oxygen consumption and ATP synthesis rates) were studied in saponin-permeabilized fibers as described [3, 4, 26], and in mitochondria isolated by differential centrifugation [27] (see supplementary methods). Substrates used were: 5 mmol/l glutamate and 2 mmol/l malate, 10 mmol/l pyruvate and 5 mmol/l malate, or 20 μmol/l palmitoyl-carnitine with 2 mmol/l malate. To evaluate maximal respiratory capacity of isolated mitochondria, O_2 consumption was determined in pyruvate-exposed mitochondria following treatment with oligomycin (1μg/ml) and the addition of FCCP (carbonyl cyanide p-trifluoromethoxyphenylhydrazone [0.7 μmol/l].

Mitochondrial fractionation

Isolated mitochondria were resuspended in 100μl 10 mmol/l Tris/HCl (pH 8.5) and subjected to 3 freeze-thaw cycles using liquid nitrogen. Lysed mitochondria were centrifuged twice at 40,000×g for 20 min at 4°C. The supernatant (matrix fraction) and the pellet (membrane fraction) were stored/suspended in 10 mmol/l Tris/HCl and maintained at −80°C until used for proteome analysis by mass spectroscopy or Blue native-PAGE (membranes only). The fractionation protocol yields a matrix fraction and a membrane fraction (containing outer and inner mitochondrial membranes) that are enriched for respective representative proteins, with minimal cross contamination (supplementary Figure S1).

Blue-native gel electrophoresis (BN-PAGE) and in-gel complex activities—BN-PAGE was performed as described [28], with some modifications (see supplementary methods).

Mitochondrial Proteomics by Mass Spectrometry

Identification of differentially expressed mitochondrial matrix and membrane proteins was achieved using liquid chromatography and mass spectroscopy (LC/MS/MS). Samples were initially subjected to tryptic digestion prior to LC and parallel fragmentation MS. (See supplementary methods).

Hydrogen peroxide (H_2O_2) measurement

Mitochondrial H_2O_2 generation was measured as previously described [4] except that palmitoyl-carnitine 60 μmol/l and L-carnitine 2 mmol/l were used as substrates.

Treatment of mice with the anti-oxidant (MnTBAP)

Four groups of mice were treated starting at 4-weeks of age. Wild-type and CIRKO mice (n = 12 per group) received twice-weekly intraperitoneal injections (20 mg/kg bodyweight) of the cell-permeable superoxide dismutase (SOD) mimetic and peroxynitrite scavenger MnTBAP (Mn (III) tetrakis (4-benzoic acid) porphyrin Chloride) (EMD Chemicals Inc. San Diego, CA) for 4 weeks. Control wild-type and CIRKO mice (n = 12 per group) received twice-weekly intraperitoneal injections of saline. After treatment, animals were euthanized and hearts collected for determination of aconitase activity and oligomycin-insensitive respiration rates.

Western blot analysis

Western-blot analysis was performed using total heart or mitochondrial proteins as previously described (see supplementary methods) [3].

Gene expression

Total RNA was extracted from ~ 30mg heart tissue with Trizol reagent (Invitrogen Corporation, Carlsbad, CA) and purified with the RNEasy Kit (Qiagen Inc., Valencia, CA). Equal amounts of heart RNA from six mice were subjected to real-time PCR using an ABI Prism 7900HT instrument (Applied Biosystems, Foster City, CA) in 384-well plate format with SYBR Green I chemistry and ROX internal reference (Invitrogen) as previously described [4, 25]. All reactions were performed in triplicate. Data were normalized to cyclophilin (CPHN). See Supplementary Table S1 for Primer sequences.

Electron Microscopy

Ventricular samples were analyzed by electron microscopy and mitochondrial volume density and number determined by stereology in a blinded fashion using the point counting method as previously described [4, 29]. For volume density, 2 images per sample were analyzed (magnification 2,000X), using 2 grids per image. For mitochondrial number, 3 images per sample were analyzed (magnification 8,000X).

Statistical Analysis

Data are means ± SEM. Comparisons of a single variable in ≥ 2 age-matched groups were analyzed by one way ANOVA followed by Fisher's least protected squares test (StatView 5.0.1 software, SAS Institute, Cary, NC). In analyses comparing ≥ 2 variables such mitochondrial parameters in control and KO mice as a function of age, a general linear model (e.g. 2-way ANOVA) was used. When significant differences existed across multiple ages, a Tukey-Kramer multiple-comparison adjustment was performed on post-hoc comparisons to determine at which ages the measures are different (SAS 9.0.3 software, SAS Institute, Cary, NC). For all analyses $p < 0.05$ was considered significant. Unless specified, p values indicate statistically significant difference between groups across all ages. When differences (by post-hoc analysis) exist between ages these will be indicated in the figure legends. Proteomic data were analyzed using previously published algorithms.[30] in brief, the key algorithm in the Waters Protein Expression System is the clustering algorithm, which chemically clusters peptide components by mass and retention time for all injected samples and performs binary comparisons for each experimental condition to generate an average normalized intensity ratio for all matched AMRT (Accurate Mass, Retention Time) components. The Student's *t*-test was used for each binary comparison.

RESULTS

Cardiac function

Cardiac function was determined by echocardiography and in isolated hearts. We previously reported that fractional shortening (%FS) and +dP/dt (*in vivo*) were reduced by 20 and 30% respectively in 10-week-old CIRKO mice [25]. Thus we determined *in vivo* cardiac function at later ages. Fractional shortening was reduced by 17% and 7% respectively in CIRKO hearts relative to controls at 27 and 67-weeks of age (Table 1). In glucose-perfused Langendorff hearts functional parameters declined with age in CIRKO and control hearts. However, developed pressure, rate pressure product (RPP) and cardiac efficiency were always signigicantly reduced in CIRKO hearts at the three ages examined (8, 24 and 54-weeks) (Table 2). Differences in cardiac function between 8-week-old CIRKO and control mice were accentuated under conditions of calcium-induced inotropic stress (Supplementary Figure S2).

Mitochondrial Dysfunction in CIRKO Mice

Mitochondrial oxygen consumption and ATP production rates in cardiac fibers from 8-, 24- and 54-week-old CIRKO mice were examined. With glutamate as substrate, maximal ADP-stimulated mitochondrial respirations (V_{ADP}) progressively declined with age (Figure 1A). At 8-weeks, CIRKO mice exhibited reduced V_{ADP} with pyruvate, which persisted up to 54 weeks, and was associated with lower ATP synthesis rates in older animals (24 to 54 weeks) (Figure 1B and H). With palmitoyl-carnitine (PC), V_{ADP}, was initially increased in 8-week-old mice, but progressively declined with age (Figure 1C). The increased PC respirations at 8-weeks was not associated with increased ATP synthesis rates (Figure 1I). By 24-weeks, ATP synthesis rates declined by 60% and the ATP/O ratio declined by 50% compared to controls (Figure 1I). Thus mitochondria from CIRKO hearts manifest 2 distinct functional defects: (^{1}) reduced respiratory capacity and ATP generation with all substrates, and (^{2}) evidence for mitochondrial uncoupling (decreased ATP/O) when exposed to a FA substrate.

To confirm the existence of FA–induced mitochondrial uncoupling, studies with pyruvate or PC-treated isolated mitochondria from 24-week-old mice were performed (Figure 2 A–D and Supplementary Figure S3). Respiration rates in isolated mitochondria are approximately 10-fold higher than in permeabilized fibers. Under these conditions the reduction in pyruvate respirations was no longer apparent in CIRKO mitochondria and there were no differences in oligomycin – insensitive (V_{oligo}) respiration or respiratory control ratios (RCR). In contrast, in the presence of the FA substrate PC, V_{oligo} was increased by 1.3-fold and the RCR was proportionately reduced by 33%. Moreover, ATP and ATP/O ratios were reduced, supporting the existence of FA-induced mitochondrial uncoupling.

To determine if reduced electron transport chain (ETC) function accounted for mitochondrial respiratory impairment, oligomycin-treated mitochondria were maximally stimulated by exposure to an uncoupling agent FCCP. Under these conditions oxygen consumption rates are independent of ATP synthesis and reflect maximal ETC capacity. There were no differences between 24-week-old CIRKO and control mitochondria (Supplementary Figure S3). We independently determined in-gel complexes I, IV and V activities, following separation of mitochondrial membrane proteins by blue-native gel electrophoresis. No differences in ETC activity were observed at any age (Figures 2 E–G).

Mitochondrial Proteins, Gene Expression and Mitochondrial Enzyme Activities

We also tested the hypothesis that defective mitochondrial function may result from changes in the content or activity of enzymes involved in intermediary mitochondrial metabolism that provide reducing equivalents to ETC. First, we conducted a proteome expression analysis of mitochondrial membrane and matrix compartments (Table 3 A, B and supplementary table

S2A, B). 93 mitochondrial matrix and 151 mitochondrial membrane proteins were identified. In the mitochondrial matrix, 24 proteins were reduced in CIRKO mice relative to controls. Of these proteins, 10 were involved in FA oxidation, 10 were involved in the TCA cycle and 3 represented subunits of pyruvate dehydrogenase (PDH) (specifically the E1 subunit and the lipoamide beta subunit). In contrast, only 10 largely unrelated proteins were increased in the matrix compartment (Table 3A, B and Supplementary Table S2A, B). In the mitochondrial membrane fraction, FA oxidation proteins were also coordinately reduced, but the pattern for OXPHOS proteins was more variable. For example, protein subunits of complex I, IV and V were increased, whereas Cytochrome C isoforms and subunits of complex III were reduced.

Second, we examined enzyme activities as a function of age, focusing on the TCA enzyme citrate synthase (CS), and the FAO regulatory enzymes, carnitine palmitoyl transferase-1 (CPT1) and 3-HydroxyAcyl-CoA dehydrogenase (HADH). Relative to age-matched controls, CS activity progressively declined with age in CIRKO mice (Supplementary Figure S4). Similarly, CPT1 and HADH activities, which were slightly enhanced at 8 weeks, also declined with age in CIRKO mice relative to their age matched controls (Supplementary Figure S4).

Third, we conducted a focused analysis of the expression of nuclear-encoded mitochondrial genes and confirmed global reduction in expression of genes involved in cellular and mitochondrial FA uptake and beta-oxidation and reduced expression of their transcriptional regulator PPAR-α (Table 4, and supplementary Figure S5). The mRNA of the E1α1 subunit of PDH was reduced by 27%. In contrast, genes that regulate mitochondrial biogenesis were essentially unaltered with the exception of SIRT1 (a potential regulator of PGC-1α activity) whose expression was reduced by 31%. Consistent with the proteomic analysis, expression of the subunit of complex III (Uqcrc1) was reduced by 20–30% ($P < 0.05$), whereas the expression of the complex I subunit (Ndufa9) was not statistically different from controls. Uncoupling protein expression (UCP2 and UCP3) was not increased, despite evidence of mitochondrial uncoupling. Pyruvate dehydrogenase kinase (PDK4) expression was reduced in 8- and 24-week old mice remdering it unlikely that reduced pyruvate flux resulted from increased phosphorylation of the E1 subunit of the PDH complex. This was confirmed by blotting for phosphorylated PDHE1, which was not altered in CIRKO hearts (Supplementary Figure S6).

Contribution of Increased Oxidative Stress to Mitochondrial Phenotypes of CIRKO Mice

To test the hypothesis that oxidative stress contributed to mitochondrial dysfunction and mitochondrial uncoupling, we measured H_2O_2 generation and the activity of mitochondrial aconitase, whose activity is susceptible to oxidative stress [31]. Mitochondrial Aconitase activity was reduced by 38% and 47% in 8- and 24-week-old CIRKO mice respectively (Figure 3A), in the absence of proportionate differences in aconitase protein levels (data not shown). H_2O_2 production was increased by 15% and 28% in 8 and 24-week-old CIRKO mice respectively versus age-matched controls (Figure 3B), following exposure to PC. Manganese superoxide dismutase (Mn-SOD) and catalase protein expression were not significantly different between CIRKO and wild-type mice at 8 weeks (data not shown). These data support the hypothesis that increased mitochondrial ROS production could be an early or primary defect in CIRKO mitochondria.

To test the hypothesis that reactive oxygen species may contribute to the increased uncoupling in 8 week-old CIRKO (as evidenced by increased V_{ADP} without an accompanying increase in ATP synthesis and increased oligomycin-insensitive respirations -V_{Oligo}), we treated CIRKO mice with the superoxide dismutase mimetic (MnTBAP) for 4 weeks starting at 4-weeks of age. Treatment with MnTBAP reversed the decline in aconitase activity both in the cytosolic (data not shown) and mitochondrial fractions (Figure 3C) and prevented the increase in V_{Oligo} in cardiac fibers from 8 week-old CIRKO mice (Figure 3D). These data suggest that ROS may be partially responsible for mitochondrial uncoupling in CIRKO mouse hearts.

Insulin Signal Transduction

PI3K signaling modulates mitochondrial FA oxidative capacity [32]. Thus we determined if differences in PI3K signaling pathways contribute to the mitochondrial phenotypes observed. CIRKO mice exhibited a significant increase in the expression of IGF-1 receptors. Moreover, there was no reduction in basal levels of Akt and GSK3β phosphorylation, which trended higher. Whereas insulin stimulation significantly increased Akt and GSK3β phosphorylation in the control hearts, no statistical increase in either Akt or GSK3β phosphorylation following perfusion of CIRKO hearts with 1nM insulin was observed (Supplementary Figure S7).

Mitochondrial Number and Ultrastructure are Altered in CIRKO Mice

Mitochondrial morphology was normal in younger CIRKO mouse hearts but at 54 weeks they appeared dysmorphic with reduced crista density (Figure 4A). Mitochondrial number and volume density were increased at all ages examined (Figure 4 B, C). These changes occurred despite the absence of any increase in expression of genes involved in mitochondrial biogenesis and mitochondrial DNA replication such as peroxisome proliferator activated receptor gamma co-activators α and β (PGC1α, PGC1β) and nuclear respiratory factors (NRF1 or NRF2). Indeed, Transcription factor A-mitochondrial (TFAM) expression was reduced in 3-week-old mice (Table 4).

DISCUSSION

Perinatal loss of insulin signaling in cardiomyocytes impairs mitochondrial function. There is an early defect in pyruvate utilization and progressive reduction in mitochondrial oxidative capacity and ATP synthesis with glutamate and palmitoyl carnitine substrates. There is a modest decline in cardiac contractility at an early age, which does not progress to heart failure, however cardiac function was significantly impaired *in vitro* following calcium-induced inotropic stress. Two mechanisms for mitochondrial dysfunction were identified. First, there was a coordinate reduction in TCA and FA enzymes that presumably impaired the delivery of reducing equivalents to the electron transport chain, which remained functionally competent. Second, mitochondria from insulin receptor deficient myocytes were more susceptible to FA-induced oxidative stress and mitochondrial uncoupling. These changes promote a mitochondrial biogenic response that occurs in the absence of increased PGC-1α expression. These data identify an important role for insulin signaling pathways in modulating mitochondrial bioenergetics and integrity. We recently reported that PI3K signaling regulates mitochondrial function in the heart [32]. The present study now shows that insulin signaling *per se* also regulates myocardial mitochondrial oxygen consumption and ATP synthesis rates. The blunted activation of PI3K targets such as Akt and its downstream substrate GSK3β in insulin-perfused CIRKO hearts is consistent with the hypothesis that reduced PI3K signaling could contribute to mitochondrial dysfunction in CIRKO hearts. However, given that basal levels of phosphorylation of these kinases were not reduced, it is also likely that PI3K or Akt – independent signals downstream of the insulin receptor also play an important role.

The mitochondrial defect appears initially to be specific for pyruvate utilization and subsequently for FA utilization. These observations provide a mechanistic basis for our previously published observations that in isolated perfused working hearts from 16–20- week-old CIRKO mice, rates of glucose and FA oxidation were both reduced [23]. An important mechanism for reduced pyruvate flux appears to be reduced content of two key subunits of the pyruvate dehydrogenase complex. The E1-alpha subunit is a key regulator of PDH flux and is the substrate of the regulatory kinase PDK4 [33, 34]. We provide novel evidence that the E1α1 subunit of PDH may be an insulin-regulated transcript in the heart, and that reduced protein levels of this subunit in mitochondrial matrix might occur on the basis of transcriptional repression. Increased phosphorylation of the E1-alpha subunit by PDK4, decreases its stability,

while blocking degradation of the E1-alpha subunit of PDH increases the activity of and flux through the enzyme complex [35]. However PDHE1 phosphorylation was not increased in CIRKO hearts and the expression of its kinase (PDK4) was actually reduced. Mitochondrial dysfunction in CIRKO mice is associated with modest reduction in cardiac function. We previously reported that cardiac function was reduced in isolated working hearts that were perfused with glucose and FA as substrates under normal workload [23]. In the present study we chose to study glucose perfused hearts because of the defect in pyruvate utilization in mitochondria. We reasoned that in the presence of glucose alone, contractile dysfunction following calcium-induced inotropic stress would be amplified.

We speculate that an early defect in glucose/pyruvate metabolism could initially lead to the increase in FA utilization that was observed in the mitochondria of 8-week-old CIRKO mice. However, this cannot be sustained over time because of the coordinate reduction in levels of mitochondrial beta-oxidation enzymes. This hypothesis is also supported by the observation of increased rates of FA oxidation (FAO) in isolated working hearts obtained from 8-week-old CIRKO mice (see supplementary Figure S8) but reduced FAO in 16–20-week-old mice [23]. The reduction in gene and protein expression levels of a broad array of regulators of FA metabolism was striking, and extends our previously reported findings that demonstrated reduced mRNA for acyl CoA dehydrogenases. The likely mechanism for these changes is insulin-mediated regulation of expression levels of the PPAR-α gene in the heart.

The second major mechanism that contributed to mitochondrial dysfunction is oxidative stress and ROS-mediated mitochondrial dysfunction. Increased ROS production was evident in the hearts of 8-week-old CIRKO mice and was sufficient to reduce the activity levels of the redox sensitive enzyme aconitase. This increase in ROS, also likely reduced mitochondrial energetics by promoting mitochondrial uncoupling as evidenced by reduced ATP/O ratios in palmitoyl carnitine treated mitochondria and increased oligomycin-insensitive respiration rates that were normalized by treating animals with the antioxidant MnTBAP. MnTBAP reduces ROS but could increase H_2O_2 generation, underscoring that mitochondrial superoxide likely mediates the changes observed. Increased ROS could reflect changes in superoxide generation or detoxification. Although, increased FA flux could contribute to increased ROS production in 8-week-old CIRKO hearts it is unlikely to represent the mechanism in older hearts in which FA oxidation is reduced. Proteomic analysis revealed changes in stoichiometry of ETC subunits, which could potentially contribute to increased superoxide generation. A major role for a reduction in ROS degradation pathways as a contributor to increased H_2O_2 production in CIRKO mitochondria appears unlikely, as neither MnSOD levels nor catalase content were changed in 8-week-old mice and in 24-week-old animals, catalase content was marginally lower. However it is possible that reduced TCA flux could limit the supply of reducing equivalents to replenish NADPH pools that maintain antioxidants such as glutathione in the reduced state. Taken together, deficient insulin signaling in the heart likely promotes mitochondrial oxidative stress by multiple mechanisms.

Mitochondrial biogenesis has been described in the hearts of insulin resistant mice and has been attributed to activation of PGC-1α-mediated signaling [36]. Here we show that mitochondrial number and volume density increased in CIRKO mice despite the lack of coordinate changes in mRNA levels of key regulators of the mitochondrial biogenesis pathway such as PGC-1α. Thus, the possibility exists that this proliferative response in CIRKO hearts is a consequence of reduced ATP generation or increased oxidative stress that promote mitochondrial biogenesis. In this regard it is important to discuss the discrepancy between citrate synthase (CS) activities and increased mitochondrial volume density in aging CIRKO mice. CS activity is widely used as an indirect estimate of mitochondrial mass. However, in CIRKO mice, our proteomic analyses indicate CS protein content in mitochondrial matrix was already significantly lower in 8-week-old CIRKO mice. This observation therefore supports

the notion that the morphological “biogenic” response that we observed represents an adaptation to pre-existing mitochondrial dysfunction in this model.

In conclusion, we demonstrate that insulin signaling is a regulator of mitochondrial oxidative capacity via mechanisms that may determine TCA cycle flux and the mitochondrial metabolism of pyruvate and fatty acids. Moreover, impaired insulin signaling predisposes cardiac mitochondria to oxidative stress, which not only might damage mitochondria, but also impairs energetics by activating mitochondrial uncoupling. Thus insulin signaling plays an essential role in the maintenance of mitochondrial homeostasis in the heart. Given the perinatal timing of insulin receptor deletion in CIRKO hearts, it is important to note that metabolic maturation of the heart continues to occur throughout the neonatal period, thus we cannot rule out that the phenotypes that we have observed might reflect unique effects of insulin resistance during this important developmental window. Future studies in mice with inducible KO of insulin receptors in adult hearts will be required to clarify this.

Diabetes and obesity are independent risk factors for the development of heart failure [37]. There is a growing body of evidence that acquired defects in insulin signaling, which may impair cardiac metabolism and are associated with LV dysfunction, develop in the heart in diabetes and obesity [38]. The present study provides new insights into potential mechanisms linking impaired post-natal insulin signaling with the development of mitochondrial dysfunction in the heart.

Supplementary Material

Refer to Web version on PubMed Central for supplementary material.

ACKNOWLEDGMENTS

We thank James Metherall Ph.D. for use of robotic facilities for gene expression analysis.

SOURCES OF FUNDING

This work was supported by grants RO1HL070070, R21DK073590 (funded by the office of Dietary Supplements and the NIDDK), UO1HL70525, and UO1HL087947 from the National Institutes of Health, 19-2006-1071 from the Juvenile Diabetes Research Foundation (JDRF) to E. Dale Abel who is an Established Investigator of the American Heart Association and the Department of Veterans Affairs to S.E. Litwin. S. Boudina was supported by postdoctoral fellowships from the JDRF and the American Heart Association (AHA). H. Bugger was supported by a postdoctoral fellowship of the German Research Foundation (DFG). V. G. Zaha is supported by a postdoctoral fellowship from the AHA, B. T. O’Neill by a physician scientist-training award from the American Diabetes Association and Eric Palfreyman by a summer research grant from the Endocrine Society.

REFERENCES

1. Boudina S, Abel ED. Mitochondrial uncoupling: a key contributor to reduced cardiac efficiency in diabetes. Physiology (Bethesda) 2006;21:250–258. [PubMed: 16868314]
2. Boudina S, Abel ED. Diabetic cardiomyopathy revisited. Circulation 2007;115:3213–3223. [PubMed: 17592090]
3. Boudina S, Sena S, O'Neill BT, Tathireddy P, Young ME, Abel ED. Reduced mitochondrial oxidative capacity and increased mitochondrial uncoupling impair myocardial energetics in obesity. Circulation 2005;112:2686–2695. [PubMed: 16246967]
4. Boudina S, Sena S, Theobald H, Sheng X, Wright JJ, Hu XX, Aziz S, Johnson JI, Bugger H, Zaha VG, Abel ED. Mitochondrial energetics in the heart in obesity-related diabetes: direct evidence for increased uncoupled respiration and activation of uncoupling proteins. Diabetes 2007;56:2457–2466. [PubMed: 17623815]
5. Bugger H, Boudina S, Hu XX, Tuinei J, Zaha VG, Theobald HA, Yun UJ, McQueen AP, Wayment B, Litwin SE, Abel ED. Type 1 Diabetic Akita Mouse Hearts are Insulin Sensitive but Manifest

Structurally Abnormal Mitochondria that Remain Coupled Despite Increased Uncoupling Protein 3. Diabetes 2008;57:2924–2932. [PubMed: 18678617]

6. Peterson LR, Herrero P, Schechtman KB, Racette SB, Waggoner AD, Kisrieva-Ware Z, Dence C, Klein S, Marsala J, Meyer T, Gropler RJ. Effect of obesity and insulin resistance on myocardial substrate metabolism and efficiency in young women. Circulation 2004;109:2191–2196. [PubMed: 15123530]
7. Scheuermann-Freestone M, Madsen PL, Manners D, Blamire AM, Buckingham RE, Styles P, Radda GK, Neubauer S, Clarke K. Abnormal cardiac and skeletal muscle energy metabolism in patients with type 2 diabetes. Circulation 2003;107:3040–3046. [PubMed: 12810608]
8. Liang Q, Carlson EC, Donthi RV, Kralik PM, Shen X, Epstein PN. Overexpression of metallothionein reduces diabetic cardiomyopathy. Diabetes 2002;51:174–181. [PubMed: 11756338]
9. Shen X, Zheng S, Metreveli NS, Epstein PN. Protection of cardiac mitochondria by overexpression of MnSOD reduces diabetic cardiomyopathy. Diabetes 2006;55:798–805. [PubMed: 16505246]
10. Shen X, Zheng S, Thongboonkerd V, Xu M, Pierce WM Jr, Klein JB, Epstein PN. Cardiac mitochondrial damage and biogenesis in a chronic model of type 1 diabetes. Am J Physiol Endocrinol Metab 2004;287:E896–E905. [PubMed: 15280150]
11. Ye G, Metreveli NS, Ren J, Epstein PN. Metallothionein prevents diabetes-induced deficits in cardiomyocytes by inhibiting reactive oxygen species production. Diabetes 2003;52:777–783. [PubMed: 12606520]
12. Desrois M, Sidell RJ, Gauguier D, King LM, Radda GK, Clarke K. Initial steps of insulin signaling and glucose transport are defective in the type 2 diabetic rat heart. Cardiovasc Res 2004;61:288–296. [PubMed: 14736545]
13. Mazumder PK, O'Neill BT, Roberts MW, Buchanan J, Yun UJ, Cooksey RC, Boudina S, Abel ED. Impaired cardiac efficiency and increased fatty acid oxidation in insulin-resistant ob/ob mouse hearts. Diabetes 2004;53:2366–2374. [PubMed: 15331547]
14. Ouwens DM, Boer C, Fodor M, de Galan P, Heine RJ, Maassen JA, Diamant M. Cardiac dysfunction induced by high-fat diet is associated with altered myocardial insulin signalling in rats. Diabetologia 2005;48:1229–1237. [PubMed: 15864533]
15. Ouwens DM, Diamant M, Fodor M, Habets DD, Pelsers MM, El Hasnaoui M, Dang ZC, van den Brom CE, Vlasblom R, Rietdijk A, Boer C, Coort SL, Glatz JF, Luiken JJ. Cardiac contractile dysfunction in insulin-resistant rats fed a high-fat diet is associated with elevated CD36-mediated fatty acid uptake and esterification. Diabetologia 2007;50:1938–1948. [PubMed: 17639306]
16. Park SY, Cho YR, Kim HJ, Higashimori T, Danton C, Lee MK, Dey A, Rothermel B, Kim YB, Kalinowski A, Russell KS, Kim JK. Unraveling the temporal pattern of diet-induced insulin resistance in individual organs and cardiac dysfunction in C57BL/6 mice. Diabetes 2005;54:3530–3540. [PubMed: 16306372]
17. Abel ED. Glucose transport in the heart. Front Biosci 2004;9:201–215. [PubMed: 14766360]
18. Brownsey RW, Boone AN, Allard MF. Actions of insulin on the mammalian heart: metabolism, pathology and biochemical mechanisms. Cardiovasc Res 1997;34:3–24. [PubMed: 9217868]
19. Slot JW, Geuze HJ, Gigengack S, James DE, Lienhard GE. Translocation of the glucose transporter GLUT4 in cardiac myocytes of the rat. Proc Natl Acad Sci U S A 1991;88:7815–7819. [PubMed: 1881917]
20. Watanabe T, Smith MM, Robinson FW, Kono T. Insulin action on glucose transport in cardiac muscle. J Biol Chem 1984;259:13117–13122. [PubMed: 6386808]
21. Lawson JW, Uyeda K. Effects of insulin and work on fructose 2,6-bisphosphate content and phosphofructokinase activity in perfused rat hearts. J Biol Chem 1987;262:3165–3173. [PubMed: 2950095]
22. Stavinoha MA, RaySpellicy JW, Essop MF, Graveleau C, Abel ED, Hart-Sailors ML, Mersmann HJ, Bray MS, Young ME. Evidence for mitochondrial thioesterase 1 as a peroxisome proliferator-activated receptor-alpha-regulated gene in cardiac and skeletal muscle. Am J Physiol Endocrinol Metab 2004;287:E888–E895. [PubMed: 15292030]
23. Belke DD, Betuing S, Tuttle MJ, Graveleau C, Young ME, Pham M, Zhang D, Cooksey RC, McClain DA, Litwin SE, Taegtmeyer H, Severson D, Kahn CR, Abel ED. Insulin signaling coordinately

regulates cardiac size, metabolism, and contractile protein isoform expression. The Journal of clinical investigation 2002;109:629–639. [PubMed: 11877471]

24. Hu P, Zhang D, Swenson L, Chakrabarti G, Abel ED, Litwin SE. Minimally invasive aortic banding in mice: effects of altered cardiomyocyte insulin signaling during pressure overload. American journal of physiology 2003;285:H1261–H1269. [PubMed: 12738623]
25. Sena S, Rasmussen IR, Wende AR, McQueen AP, Theobald HA, Wilde N, Pereira RO, Litwin SE, Berger JP, Abel ED. Cardiac hypertrophy caused by peroxisome proliferator- activated receptor-gamma agonist treatment occurs independently of changes in myocardial insulin signaling. Endocrinology 2007;148:6047–6053. [PubMed: 17823261]
26. Veksler VI, Kuznetsov AV, Sharov VG, Kapelko VI, Saks VA. Mitochondrial respiratory parameters in cardiac tissue: a novel method of assessment by using saponin-skinned fibers. Biochim Biophys Acta 1987;892:191–196. [PubMed: 3593705]
27. Rolfe DF, Hulbert AJ, Brand MD. Characteristics of mitochondrial proton leak and control of oxidative phosphorylation in the major oxygen-consuming tissues of the rat. Biochim Biophys Acta 1994;1188:405–416. [PubMed: 7803454]
28. Wittig I, Braun HP, Schagger H. Blue native PAGE. Nat Protoc 2006;1:418–428. [PubMed: 17406264]
29. Weibel ER. Stereological principles for morphometry in electron microscopic cytology. Int Rev Cytol 1969;26:235–302. [PubMed: 4899604]
30. Silva JC, Denny R, Dorschel CA, Gorenstein M, Kass IJ, Li GZ, McKenna T, Nold MJ, Richardson K, Young P, Geromanos S. Quantitative proteomic analysis by accurate mass retention time pairs. Analytical chemistry 2005;77:2187–2200. [PubMed: 15801753]
31. Fillebeen C, Pantopoulos K. Redox control of iron regulatory proteins. Redox Rep 2002;7:15–22. [PubMed: 11981450]
32. O'Neill BT, Kim J, Wende AR, Theobald HA, Tuinei J, Buchanan J, Guo A, Zaha VG, Davis DK, Schell JC, Boudina S, Wayment B, Litwin SE, Shioi T, Izumo S, Birnbaum MJ, Abel ED. A conserved role for phosphatidylinositol 3-kinase but not Akt signaling in mitochondrial adaptations that accompany physiological cardiac hypertrophy. Cell Metab 2007;6:294–306. [PubMed: 17908558]
33. Harris RA, Bowker-Kinley MM, Huang B, Wu P. Regulation of the activity of the pyruvate dehydrogenase complex. Adv Enzyme Regul 2002;42:249–259. [PubMed: 12123719]
34. Sugden MC, Holness MJ. Recent advances in mechanisms regulating glucose oxidation at the level of the pyruvate dehydrogenase complex by PDKs. Am J Physiol Endocrinol Metab 2003;284:E855–E862. [PubMed: 12676647]
35. Morten KJ, Caky M, Matthews PM. Stabilization of the pyruvate dehydrogenase E1alpha subunit by dichloroacetate. Neurology 1998;51:1331–1335. [PubMed: 9818855]
36. Duncan JG, Fong JL, Medeiros DM, Finck BN, Kelly DP. Insulin-resistant heart exhibits a mitochondrial biogenic response driven by the peroxisome proliferator-activated receptor-alpha/PGC-1alpha gene regulatory pathway. Circulation 2007;115:909–917. [PubMed: 17261654]
37. Abel ED. Myocardial insulin resistance and cardiac complications of diabetes. Curr Drug Targets Immune Endocr Metabol Disord 2005;5:219–226. [PubMed: 16089356]
38. Abel ED, Litwin SE, Sweeney G. Cardiac remodeling in obesity. Physiological reviews 2008;88:389–419. [PubMed: 18391168]

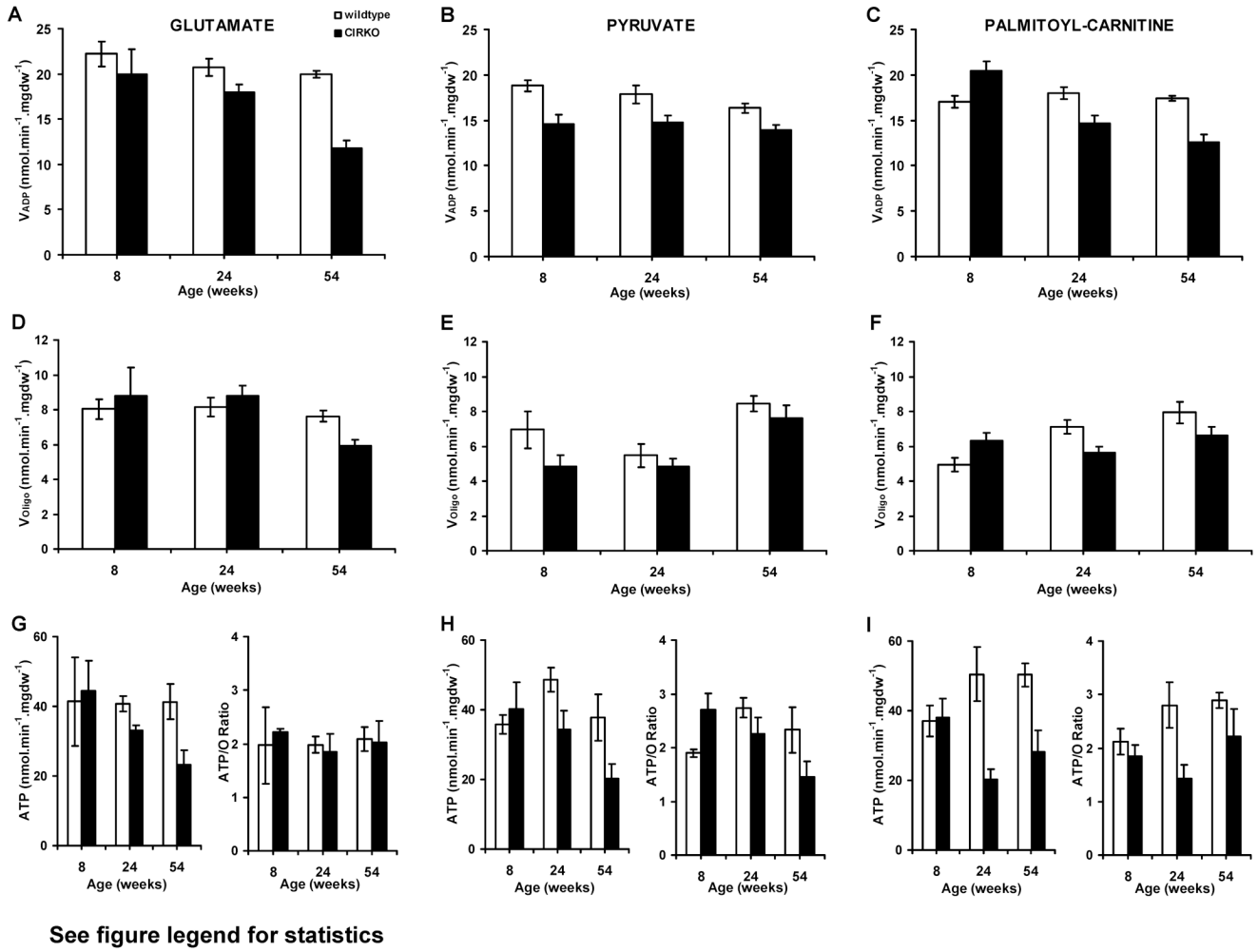

Figure 1. Age-dependent changes in mitochondrial respiration and ATP synthesis rates in CIRKO and wild-type mice

(Data are means±SEM).

(A), (D) and **(G)**: V_{ADP}, V_{Oligo}, ATP synthesis rates and ATP/O ratio in the presence of glutamate-malate in 8- (n=4), 24- (n=4) and 54- (n=5) week-old CIRKO (black bars) and wild-type (WT) (white bars) respectively. Statistics (2-Way ANOVA): Panel A: V_{ADP} –WT vs. CIRKO, p<0.01, 54-weeks vs. 8-weeks, p<0.01, 24-weeks vs. 54-weeks, P=0.06. Panel D and G: No statistical differences between groups.

(B), (E), and **(H)** Same as (A), (D), (G) but in the presence of pyruvate-malate. Statistics (2-Way ANOVA): Panel B: V_{ADP} – WT vs. CIRKO, p<0.005; Panel E: V_{Oligo} – 54-weeks vs. 24 or 8-weeks, p<0.01; Panel H: ATP – WT vs. CIRKO, p<0.05.

(C), (F), and **(I)** Same as (A), (D), (G) but in the presence of palmitoyl-carnitine and malate. Statistics (2-Way ANOVA): Panel C: V_{ADP} – WT vs. CIRKO (at all ages), p<0.05, Decline in CIRKO with age (p<0.005, after multiple comparison adjustments). Panel F: V_{Oligo} – WT vs. CIRKO (at 8-weeks), p<0.005, Increase in WT with age (p<0.005, after multiple adjustments). Panel I: ATP – WT vs. CIRKO, p<0.01 and p<0.05 at 24 and 54-weeks respectively. ATP/O – WT vs. CIRKO, p<0.01.

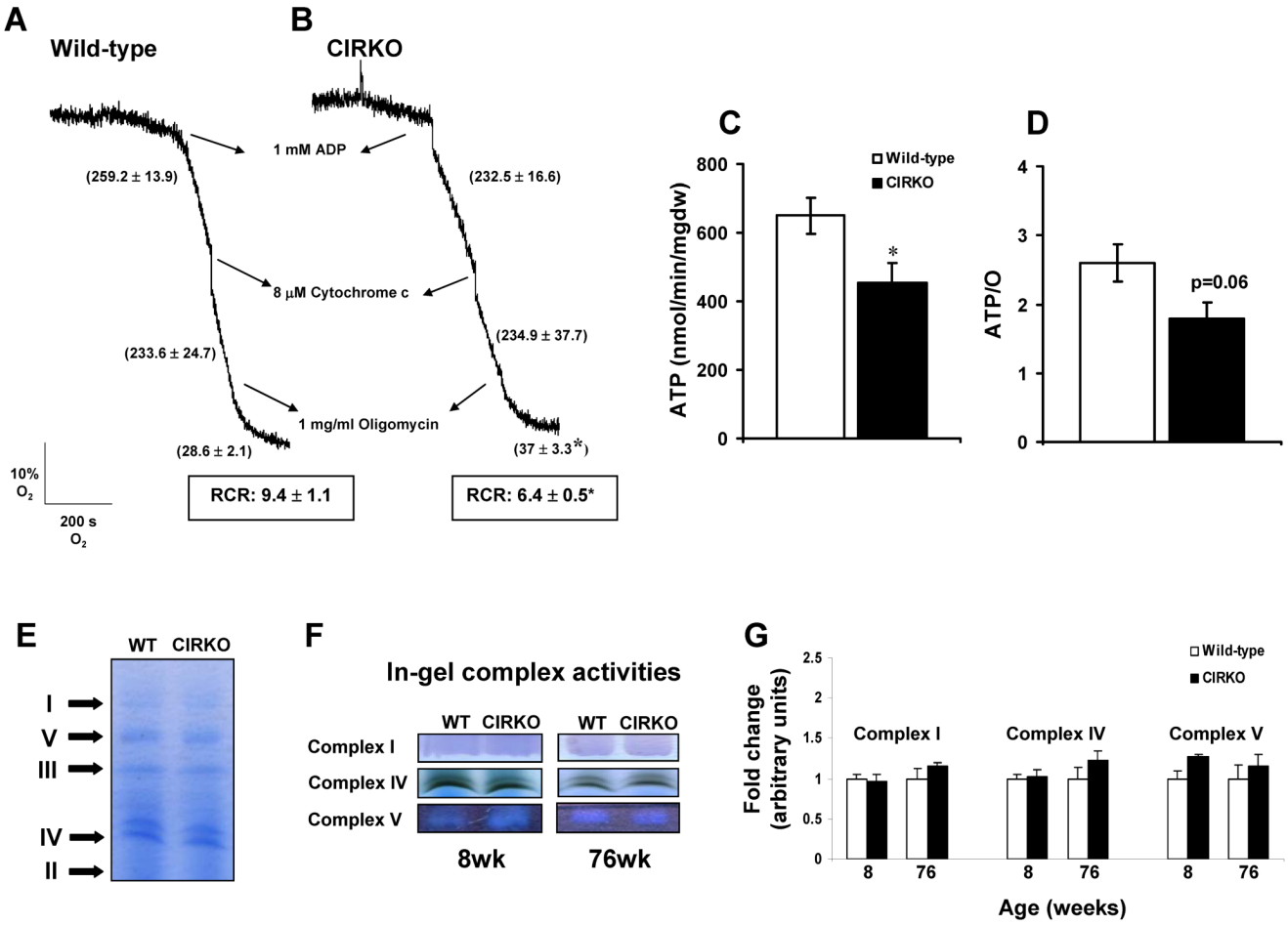

Figure 2. Mitochondrial function and electron transport chain complex activity

(A) and **(B)** Respiration traces of mitochondria (0.4 mg/ml) isolated from 24-week-old wild-type (n = 5) and CIRKO mice (n = 5) respectively, using palmitoyl-carnitine as substrate.

(C) and **(D)** ATP and ATP/O ratio (means±SEM) measured on isolated mitochondria from wild-type and CIRKO mice at 24-weeks of age using palmitoyl-carnitine as substrate.

(E) Representative blue-native polyacrylamide gel electrophoresis (BN-PAGE) Arrows indicate separation of complexes I, II, III, IV, and V.

(F) and **(G)** Representative in-gel complex activity stainings, and densitometric quantification (means±SEM) of complex I, IV, and V activities, of wild-type and CIRKO mice at 8- and 76-weeks of age (n = 4 – 5).

* $p < 0.05$ vs. age-matched wild-type controls.

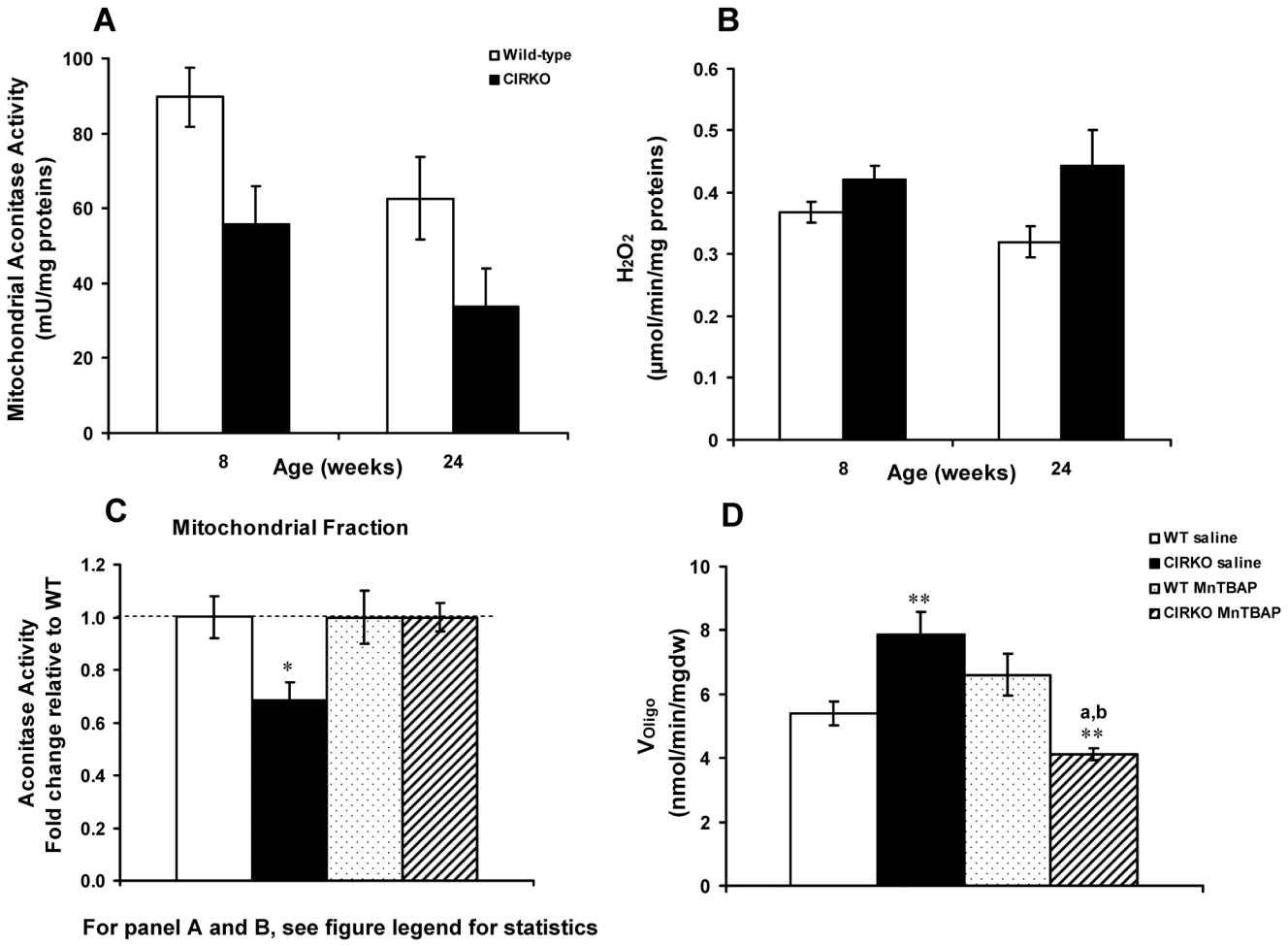

Figure 3. Increased oxidative stress in CIRKO hearts

(Data are means±SEM).

A) Aconitase activity measured in mitochondria isolated from 8- and 24-week-old CIRKO (black bars, n=5) and wild-type (white bars, n=6) hearts. Statistics (2-Way ANOVA): WT vs. CIRKO, $p<0.05$ and $p<0.005$ at 8 and 24-weeks respectively.

B) Hydrogen peroxide (H_2O_2) production in isolated mitochondria obtained from 8 and 24-week-old CIRKO (n=7) and wild-type (n=7). Mitochondria were incubated with palmitoyl-carnitine and L–carnitine in the presence of oligomycin as described in the methods. Statistics (2-Way ANOVA): WT vs. CIRKO, $p<0.005$

C) Mitochondrial aconitase activity determined in saline-treated wild-type (open bars, n=6 per group), and CIRKO mice (black bars, n=6), and MnTBAP-treated wild-type (dotted bars, n=6) and CIRKO mice (hatched bars, n=6), age 8-weeks.

D) Oligomycin-insensitive respiration ($V_{oligomycin}$) in saponin-permeabilized cardiac fibers from wild-type (saline and MnTBAP) and CIRKO mice (saline and MnTBAP), age 8-weeks. * $p<0.05$, ** $p < 0.005$ versus wild-type; [a] $p < 0.005$ versus CIRKO saline; [b] $p < 0.005$ versus wild-type MnTBAP (1-Way ANOVA).

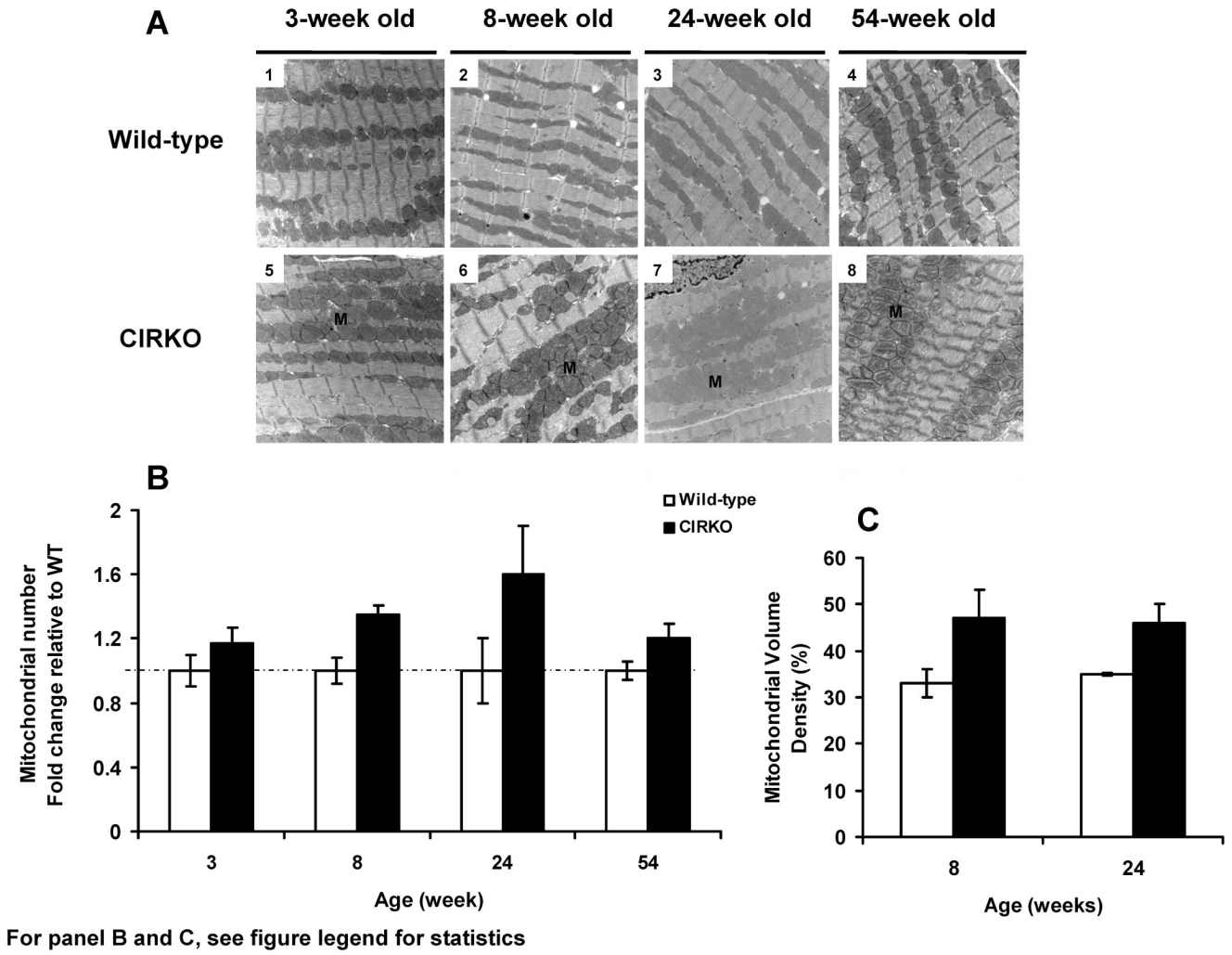

Figure 4. Mitochondrial number and morphology in CIRKO and wild-type hearts

A) Representative electron micrographs of heart sections (80–100 nm) from 3-, 8-, 24-, and 54-week-old wild-type (1, 2, 3 and 4) and CIRKO (5, 6, 7 and 8) mice (three per group).

B) Quantification of mitochondrial number in CIRKO hearts (fold change vs. wild-type normalized to 1±SEM). Statistics (2-Way ANOVA): WT vs. CIRKO, $p<0.005$.

C) Mitochondrial volume density relative to cell area in wild-type and CIRKO mice at 8- and 24-weeks of age. Statistics (2-Way ANOVA): WT vs. CIRKO, $p<0.005$.

Table 1

In-vivo cardiac function measured by echocardiography

	27 week-old		67 week-old	
	Wild-type (n=7)	*CIRKO (n=8)*	*Wild-type (n=5)*	*CIRKO (n=5)*
LVDd. (cm)[a]	0.39 ± 0.01	0.39 ± 0.007	0.42 ± 0.01	0.41 ± 0.01
LVDs. (cm)	0.27 ± 0.01	0.30 ± 0.008	0.31 ± 0.02	0.31 ± 0.006
IVSd. (cm)[b]	0.08 ± 0.004	0.07 ± 0.003	0.08 ± 0.005	0.07 (0.003
IVSs. (cm)	0.10 (0.01	0.10 (0.003	0.12 (0.008	0.10 (0.005
PWd. (cm)	0.08 (0.006	0.07 (0.003	0.08 (0.004	0.07 (0.003
PWs. (cm)	0.11 (0.004	0.10 (0.003	0.11 (0.007	0.10 (0.003
% FS[b]	29.40 (1.75	24.43 (0.91	25.95 (2.49	24.09 (1.3
EF[b]	0.64 (0.02	0.56 (0.01	0.58 (0.04	0.56 (0.02
HR. (beats/min)	455 ± 31	474 ± 15	460 ± 16	443 ± 23
SV. (ml)	0.03 ± 0.003	0.03 ± 0.002	0.04 ± 0.003	0.04 ± 0.004
CO. (ml/min)	17.29 ± 1.54	17.02 ± 0.92	20.45 ± 1.06	18.34 ± 2.22

Values are mean ± SEM.

[a] $p<0.05$, 27-week vs. 67-week (both genotypes respectively)

[b] $p<0.05$, Wild-type vs. CIRKO (both ages), by 2-way ANOVA. LVDd: left ventricular dimension in diastole; LVDs: left ventricular dimension in systole; IVSd: inter-ventricular septum in diastole; IVSs: inter-ventricular septum in systole; PWd: posterior wall of left ventricle in diastole; PWs: posterior wall of left ventricle in systole; FS: fractional shortening; EF: ejection fraction; HR: heart rate; SV: stroke volume; CO: cardiac output.

Table 2

Cardiac function, MVO_2 and cardiac efficiency in wild-type and CIRKO hearts under unstimulated conditions

	8 week-old (n=17)		24 week-old (n=19)		54 week-old (n=7)	
	Wild-type	***CIRKO***	***Wild-type***	***CIRKO***	***Wild-type***	***CIRKO***
Body weight (BW) (g) [a]	22.6 ± 0.8	21.3 ± 0.5	29.9 ± 1.1	28.1 ± 0.7	30.5± 1.3	30.5 ± 1.9
Heart weight (HW) (g) [ab]	0.14 ± 0.01	0.10 ± 0.03	0.16 ± 0.01	0.12 ± 0.01	0.17 ± 0.05	0.15 ± 0.02
HW/BW × 10^3 [b]	6.1 ± 0.2	4.7 ± 0.11	5.3 ± 0.12	4.2 ± 0.15	5.4 ± 0.1	4.8 ± 0.3
HR (beats/min)	362 ± 2	355 ± 8	349 ± 8	344 ± 9	351 ± 14	334 ± 13
DP (mmHg) [c]	12.1 ± 1.5	12.9 ± 1.7	9.6 ± 1.0	10.5 (1.2	15.4 (2.3	14.3 (1.8
SP (mmHg) [ab]	80.6 (2.7	72.2 (2.7	67 (1.9	62.8 (2.2	76.6 (5.9	57.5 (3.6
DVP (mmHg) [ab]	68.5 (2.5	59.3 (2.8	57.4 (1.7	52.3 (1.7	61.2 (5.3	43.2 (3.5
RPP × 10^3 (mmHg × beats/min) [ab]	24.8 ± 0.9	21.1 ± 1.2	20 ± 0.6	18.1 ± 0.8	21.2 ± 1.6	14.2 ± 0.8
$-dP/dt_{min.} \times 10^3$ (mmHg/s) [a]	3.3 ± 0.2	3.2 ± 0.2	2.3 ± 0.07	2.1 ± 0.07	2.6 ± 0.4	2.4 ± 0.3
$dP/dt_{max.} \times 10^3$ (mmHg/s) [a]	3.9 ± 0.3	3.6 ± 0.3	2.7 ± 0.1	2.5 ± 0.08	3.5 ± 0.5	2.8 ± 0.2
MVO_2 (µmol/min/g)	25.1 ± 1.2	24.4 ± 1.2	23.2 ± 1.2	23.7 ± 1.4	26 ± 2.2	19.4 ± 1.8
% CE [b]	29.8 ± 1.0	26 ± 1.2	26.4 ± 1.1	23.7 ± 1.5	25.6 ± 3.0	22.9 ± 2.6

Values are mean ± SEM. Statistics by 2-way ANOVA:

[a] 8-week vs. 24 and 54-weeks, $p<0.01$;

[b] Wild-type (WT) vs. CIRKO, $p < 0.01$;

[c] 24 vs. 54-weeks, $p<0.01$. HR: heart rate; DP: diastolic pressure; SP: systolic pressure; DVP: developed pressure; RPP: rate pressure product; MVO_2: myocardial oxygen consumption; CE: cardiac efficiency.

Table 3

Table 3A: Proteomic Analysis of Mitochondrial Membrane Proteins in CIRKO Mice.

Protein	Fold Change CIRKO/WT ($p<0.05$)	Pathway
solute carrier family 25 (mitochondrial carrier, adenine nucleotide translocator), member 13	1.16	ADP/ATP Translocase
solute carrier family 25 (mitochondrial carrier, phosphate carrier), member 3	1.08	ADP/ATP Translocase
solute carrier family 25, member 5	1.05	ADP/ATP Translocase
glutamate oxaloacetate transaminase 2, mitochondrial	0.92	Amino Acid metabolism/anapleurosis/TCA
PREDICTED: similar to Aspartate aminotransferase, mitochondrial precursor (Transaminase A) (Glutamate oxaloacetate transaminase 2)	0.93	Amino Acid metabolism/anapleurosis
electron transferring flavoprotein, dehydrogenase	0.86	Electron Transfer to Complex II
2,4-dienoyl CoA reductase 1, mitochondrial	0.86	FA beta-oxidation
acetyl-Coenzyme A acyltransferase 2 (mitochondrial 3-oxoacyl-Coenzyme A thiolase)	0.83	FA beta-oxidation
acetyl-Coenzyme A dehydrogenase, long-chain [Mus musculus]	1.14	FA beta Oxidation
acyl-CoA synthetase long-chain family member 1	0.87	FA beta-oxidation
acyl-Coenzyme A dehydrogenase, very long chain	0.80	FA beta-oxidation
carnitine acetyltransferase	0.79	FA beta-oxidation
carnitine palmitoyltransferase 2	0.68	FA beta-oxidation
hydroxyacyl-Coenzyme A dehydrogenase/3-ketoacyl-Coenzyme A thiolase/enoyl-Coenzyme A hydratase (trifunctional protein), alpha subunit	0.90	FA beta-oxidation
hydroxyacyl-Coenzyme A dehydrogenase/3-ketoacyl-Coenzyme A thiolase/enoyl-Coenzyme A hydratase (trifunctional protein), beta subunit	0.76	FA beta-oxidation
PREDICTED: similar to acyl-CoA synthetase long-chain family member 1 isoform 4	0.88	FA beta-oxidation
PREDICTED: similar to acyl-CoA synthetase long-chain family member 1 isoform 5	0.88	FA beta-oxidation
PREDICTED: similar to hydroxyacyl-Coenzyme A dehydrogenase/3-ketoacyl-Coenzyme A thiolase/enoyl-Coenzyme A hydratase (trifunctional protein), beta subunit	0.75	FA beta-oxidation
dihydrolipoamide S-acetyltransferase (E2 component of pyruvate dehydrogenase complex) [Mus musculus]	1.19	Glucose Oxidation
pyruvate dehydrogenase (lipoamide) beta	1.12	Glucose Oxidation
3-oxoacid CoA transferase 1 [Mus musculus]	1.23	Ketone Metabolism
Tu translation elongation factor, mitochondrial	1.2	Mitochondrial Chaperone, Mitochondrial protein translation
NADH dehydrogenase (ubiquinone) 1 alpha subcomplex, 9 [Mus musculus]	1.12	OXPHOS complex I
NADH dehydrogenase (ubiquinone) Fe-S protein 1	1.11	OXPHOS complex I
NADH dehydrogenase (ubiquinone) Fe-S protein 6	1.18	OXPHOS complex I
PREDICTED: similar to NADH dehydrogenase (ubiquinone) Fe-S protein 3	1.11	OXPHOS complex I
PREDICTED: similar to NADH dehydrogenase (ubiquinone) Fe-S protein 6	1.23	OXPHOS complex I
cytochrome c-1	0.87	OXPHOS complex III

Table 3A: Proteomic Analysis of Mitochondrial Membrane Proteins in CIRKO Mice.

Protein	Fold Change CIRKO/WT (p<0.05)	Pathway
ubiquinol cytochrome c reductase core protein 2	0.94	OXPHOS complex III
cytochrome c oxidase subunit IV isoform 1 [Mus musculus]	1.09	OXPHOS complex IV
ATP synthase, H+ transporting, mitochondrial F1 complex, alpha subunit, isoform 1	0.96	OXPHOS complex V
ATP synthase, H+ transporting, mitochondrial F1 complex, delta subunit precursor [Mus musculus]	1.08	OXPHOS complex V
ATP synthase, H+ transporting, mitochondrial F1 complex, gamma subunit [Mus musculus]	1.09	OXPHOS complex V
cytochrome c, somatic	0.87	OXPHOS cytochrome c
PREDICTED: similar to Cytochrome c, somatic	0.87	OXPHOS cytochrome c
PREDICTED: similar to Cytochrome c, somatic isoform 1	0.87	OXPHOS cytochrome c
PREDICTED: similar to Cytochrome c, somatic isoform 2	0.87	OXPHOS cytochrome c
creatine kinase, mitochondrial 1, ubiquitous	0.84	Phospho-transfer
creatine kinase, mitochondrial 2	0.76	Phospho-transfer
nicotinamide nucleotide transhydrogenase	1.23	Proton Transport and NADPH Regeneration
citrate synthase-like protein [Mus musculus]	1.12	TCA
dihydrolipoamide S-succinyltransferase (E2 component of 2-oxo-glutarate complex) [Mus musculus]	1.19	TCA
isocitrate dehydrogenase 2 (NADP+), mitochondrial [Mus musculus]	1.43	TCA
malate dehydrogenase 2, NAD (mitochondrial)	0.93	TCA
oxoglutarate dehydrogenase (lipoamide)	1.12	TCA (ROS production)
heat shock protein 9A [Mus musculus]	1.27	Unknown
hypothetical protein LOC237880 [Mus musculus]	1.16	Unknown

Table 3B: Proteomic Analysis of Mitochondrial Matrix Proteins from CIRKO Mice.

Protein	Fold Change CIRKO/WT (p<0.05)	Pathway
glutamate oxaloacetate transaminase 2, mitochondrial	0.88	Amino Acid metabolism/anapleurosis/TCA
PREDICTED: similar to Aspartate aminotransferase, mitochondrial precursor (Transaminase A) (Glutamate oxaloacetate transaminase 2)	0.88	Amino Acid metabolism/anapleurosis/TCA
acetyl-Coenzyme A acyltransferase 2 (mitochondrial 3-oxoacyl-Coenzyme A thiolase)	0.74	FA beta-oxidation
acetyl-Coenzyme A dehydrogenase, long-chain	0.89	FA beta-oxidation
acetyl-Coenzyme A dehydrogenase, medium chain	0.76	FA beta-oxidation
acyl-Coenzyme A dehydrogenase, short chain	0.71	FA beta-oxidation
acyl-Coenzyme A dehydrogenase, very long chain	1.52	FA beta-oxidation
dodecenoyl-Coenzyme A delta isomerase (3,2 trans-enoyl-Coenyme A isomerase)	0.77	FA beta-oxidation
enoyl Coenzyme A hydratase, short chain, 1, mitochondrial	0.88	FA beta-oxidation
hydroxyacyl-Coenzyme A dehydrogenase/3-ketoacyl-Coenzyme A thiolase/enoyl-Coenzyme A hydratase (trifunctional protein), beta subunit	1.37	FA beta-oxidation
L-3-hydroxyacyl-Coenzyme A dehydrogenase, short chain	0.70	FA beta-oxidation

Table 3B: Proteomic Analysis of Mitochondrial Matrix Proteins from CIRKO Mice.		
Protein	**Fold Change CIRKO/WT ($p<0.05$)**	**Pathway**
PREDICTED: similar to hydroxyacyl-Coenzyme A dehydrogenase/3-ketoacyl-Coenzyme A thiolase/enoyl-Coenzyme A hydratase (trifunctional protein), beta subunit	1.33	FA beta-oxidation
electron transferring flavoprotein, alpha polypeptide	0.89	FA metabolism
electron transferring flavoprotein, beta polypeptide	0.94	FA metabolism
thioesterase superfamily member 2	0.59	FA metabolism
PREDICTED: similar to Pyruvate dehydrogenase E1 component alpha subunit, somatic form, mitochondrial precursor (PDHE1-A type I) isoform 2	0.76	Glucose oxidation
pyruvate dehydrogenase (lipoamide) beta	0.86	Glucose oxidation
pyruvate dehydrogenase E1 alpha 1	0.75	Glucose oxidation
3-oxoacid CoA transferase 1	1.23	Ketone Metabolism
inner membrane protein, mitochondrial	1.28	(Mitofillin) Required for normal mitochondrial inner membrane morphology
PREDICTED: similar to coiled-coil-helix-coiled-coil-helix domain containing 3 isoform 2	1.28	Mitofillin binding partner
ATP synthase, H+ transporting mitochondrial F1 complex, beta subunit	1.37	OXPHOS complex V
ATP synthase, H+ transporting, mitochondrial F1 complex, alpha subunit, isoform 1	1.37	OXPHOS complex V
aconitase 2, mitochondrial	0.92	TCA
aldehyde dehydrogenase family 6, subfamily A1	0.83	TCA
citrate synthase	0.9	TCA
fumarate hydratase 1	0.92	TCA
isocitrate dehydrogenase 2 (NADP+), mitochondrial	1.06	TCA
isocitrate dehydrogenase 3 (NAD+) alpha	0.78	TCA
oxoglutarate dehydrogenase (lipoamide	0.77	TCA
PREDICTED: similar to Malate dehydrogenase, mitochondrial precursor	0.87	TCA
succinate-Coenzyme A ligase, ADP-forming, beta subunit	0.61	TCA
PREDICTED: similar to 60 kDa heat shock protein, mitochondrial precursor (Hsp60) (60 kDa chaperonin) (CPN60) (Heat shock protein 60) (HSP-60) (Mitochondrial matrix protein P1) (HSP-65)	0.8	Unknown

Table 4

Relative changes in gene expression in CIRKO and wild-type mice

	Wild-type	CIRKO 3 weeks	CIRKO 8 weeks	CIRKO 14–24 weeks
Fatty acid Metabolism				
ACADM (MCAD)	1	0.7**	0.7**	0.7*
CPT1b	1	1	0.9	0.9
CPT2	1	0.7**	0.5**	0.6**
CD36	1	0.8*	0.7*	0.7*
FABP	1	0.8**	0.7*	0.7*
PPARα	1	0.7*	0.7*	0.7
Mitochondrial Biogenesis				
PGC1α	1	N/D	1.01	1.08
PGC1β	1	N/D	0.98	0.89
(ESRRA) ERRα	1	1.4	0.6	1
TFAM	1	0.7*	1	0.9
NFR1	1	1	1	0.7
NRF2	1	0.9	1	0.8
SIRT1	1	N/D	0.69*	N/D
Oxidative Phosphorylation				
Ndufa9	1	0.8	0.9	0.8
Uqcrc1	1	0.7*	0.7*	0.8*
Others				
UCP2	1	0.9	0.9	0.9
UCP3	1	1.2	0.8	0.5**
PDK4	1	1.5	0.3*	0.6
PDHA1	1	N/D	0.72**	N/D
CKMT2 (MTCK)	1	0.7*	0.7**	0.7*
MTE1	1	0.9	0.6*	0.6*

Total RNA from six wild-type and six CIRKO hearts at each age respectively, was quantified by real-time PCR and normalized to cyclophilin expression. Values represent fold change in mRNA levels relative to wild-type, which were assigned as 1.

* $p < 0.05$;

** $p < 0.005$ *versus* age-matched wild-type controls. N/D = not done. Full gene names are in the supplementary Table S1.